Positron Scattering from the Group IIB Metals Zinc and Cadmium: Recommended Cross Sections and Transport Simulations

P. W. Stokes, R. D. White, R. P. McEachran, et al.

View Online   Export Citation   CrossMark

ARTICLES YOU MAY BE INTERESTED IN

Journal of Physical and Chemical Reference Data

READ TODAY!

CODATA Recommended Values of the Fundamental Physical Constants: 2018

Positron Scattering from the Group IIB Metals Zinc and Cadmium: Recommended Cross Sections and Transport Simulations

P. W. Stokes,[1] [ID] R. D. White,[1] [ID] R. P. McEachran,[2] F. Blanco,[3] [ID] G. García,[4] [ID] and M. J. Brunger[5,6,a)] [ID]

AFFILIATIONS

[1]College of Science and Engineering, James Cook University, Townsville, Queensland 4810, Australia
[2]Laser Physics Centre, RSP, Australian National University, Canberra, ACT 0200, Australia
[3]Departamento de Estructura de la Materia, Física Térmica y Electrónica e IPARCOS, Universidad Complutense de Madrid, Plaza de Ciencias 1, E-28040 Madrid, Spain
[4]Instituto de Física Fundamental, CSIC, Serrano 113-bis, E-28006 Madrid, Spain
[5]College of Science and Engineering, Flinders University, GPO Box 2100, Adelaide, SA 5001, Australia
[6]Department of Actuarial Science and Applied Statistics, Faculty of Business and Management, UCSI University, Kuala Lumpur 56000, Malaysia

a)Author to whom correspondence should be addressed: michael.brunger@flinders.edu.au

ABSTRACT

Results from the application of our optical potential and relativistic optical potential models to positron scattering from gas-phase zinc (Zn) and cadmium (Cd) are presented. In particular, integral cross sections (ICSs) for elastic scattering, positronium formation, summed discrete electronic-state excitation, and ionization scattering processes are reported for both species and over an extended incident positron energy range. From those ICSs, the total cross section is subsequently constructed by taking their sum. We note that there are currently no experimental data available for any of these scattering processes for either species, with earlier computational results being limited to the elastic channel and restricted to relatively narrow incident positron energy regimes. Nonetheless, we construct recommended positron cross section datasets for both zinc and cadmium over the incident positron energy range of 0–10 000 eV. The recommended positron cross section data are subsequently employed in a multi-term Boltzmann equation analysis to simulate the transport of positrons, under the influence of an applied (external) electric field, through the background Zn and Cd gases. Qualitatively similar behavior in the calculated transport coefficients was observed between both species. Finally, for the case of zinc, the present positron transport coefficients are compared against corresponding results from electron transport with some significant differences now being observed.

Published by AIP Publishing on behalf of the National Institute of Standards and Technology. https://doi.org/10.1063/5.0046091

Key words: cadmium; positron scattering cross sections; positron transport; recommended cross sections; zinc.

CONTENTS

1. Introduction

In this study, we extend our earlier work on positron scattering from the group II atoms beryllium (Be) and magnesium (Mg)[1] to now investigate the collisional behavior of positron scattering from the group IIB metals zinc (Zn) and cadmium (Cd). Previous studies on both these scattering systems have been limited, and indeed, we know of no experimental measurements[2] for any of the available scattering channels, i.e., elastic scattering, positronium (Ps) formation, discrete electronic-state excitation, and direct ionization (I), for either atom. In terms of theoretical calculations, we note relatively early cross section results for elastic scattering of positrons from cadmium by Pangantiwar and Srivastava,[3] Nahar,[4] and Szmytkowski,[5] while only Szmytkowski also considered zinc. All these studies were conducted over quite limited incident positron energy (E_0) regimes, with the calculations of Pangantiwar and Srivastava being for E_0 = 40–150 eV, those of Nahar being for E_0 = 6.4–300 eV, and finally, the results of Szmytkowski[5] being in the range $E_0 \sim$ 1–100 eV. More recently, the group originally based at Charles Darwin University (CDU)[6,7] undertook work at very low incident positron energies for both Zn and Cd. Those studies on Zn[6] and Cd[7] were primarily aimed at addressing the question of whether or not positrons could bind to them, but low-energy elastic integral cross sections (ICSs) were also reported ($E_0 \sim$ 0–10 eV). One of the significant finds from Mitroy and co-workers[6,7] was that the description of the low-energy scattering dynamics was very sensitive to the polarization potential utilized in the calculations.

One of the main rationales behind this study is to develop a complete and self-consistent ICS database,[1,8] for all relevant scattering processes and over a very wide energy range (0–10 000 eV), to enable simulations of charged-particle track behavior, in the atom or molecule of interest (e.g. Refs. 9–11), to be undertaken. In order to achieve that aim, we supplement the existing results with those from the application of our optical potential (OP) and relativistic OP models (ROPs).[1] In doing so, for the first time, we also report ICSs for positronium formation, summed discrete electronic-state excitation processes, and total ionization cross sections (TICSs). Furthermore, when each of the aforementioned cross sections is summed, at each E_0, with the elastic ICS, the grand total cross section (TCS) can be derived for each of Zn and Cd. This is no moot point as, in principle, corresponding experimental TCS could be measured on the positron beamline at The Australian National University (ANU). Measurements on condensable targets such as Zn and Cd are difficult, but in their earlier work with uracil,[12] the ANU group showed that absolute

TCS can be obtained. Indeed, we hope that the present study might stimulate the ANU group to undertake such experiments.

Another rationale behind the present investigation is to use our recommended cross section database in order to simulate[13] the transport of positrons in gaseous Zn and Cd under the influence of an applied (external) electric field. The connection between the macroscopic transport parameters [e.g., the drift velocity and diffusion coefficients as a function of the reduced electric field (E/n_0, where E = electric field strength and n_0 = number density)] and the cross sections that drive the scattering phenomena at the nanoscale is well elucidated by those simulations and forms an important gateway to characterizing low-temperature positron plasmas. Indeed, interesting physical phenomena such as negative differential conductivity (NDC),[14,15] a reduction in the mean energy (ϵ) of the positron swarm as a function of increasing E/n_0, and the plateauing of longitudinal and transverse diffusion coefficients ($D_{L,T}$) with increasing E/n_0 might be found. These are all driven by the cross sections for the relevant open scattering channels at the reduced electric fields and were found by the simulations in our work on Be and Mg,[1] and we are very interested to see if they are also prevalent here. Note, in particular, that NDC can be indicative of the existence of a Ramsauer–Townsend minimum in the TCS. However, this is more of a coincidence than a given as the underlying physics that drives these phenomena is very different in each case.

The structure of the remainder of this paper is as follows: In Sec. II, we provide details of our OP and ROP calculations, while in Sec. III these results are compared and discussed against those, for both Zn and Cd, that are currently available in the literature. On the basis of that comparison, in Sec. IV, we formulate the recommended data for those species for elastic scattering, positronium formation, the sum of all the discrete inelastic channels, ionization, and total scattering. Using those recommended positron cross section sets, in Sec. V, the results from our multi-term Boltzmann equation analysis of positron transport in Zn and Cd are presented and compared. Brief details of our simulation methodology are also given in Sec. V, as is a comparison between the present positron–Zn simulation results and those from an earlier electron–Zn study.[16] Finally, in Sec. VI, some conclusions from this investigation are outlined.

2. Theoretical Details

In this section, we provide some brief details with respect to our current OP and ROP theoretical methods and their application to positron (e^+) scattering processes.

2.1. Optical potential

Our OP method is based on a local complex potential representing the atomic scattering center, according to the equation

$$V(r) = V_s(r) + V_p(r) - iV_a(r), \tag{1}$$

where $V_s(r) + V_p(r)$ is the real, or elastic, scattering part of the OP and $iV_a(r)$ is the imaginary absorption potential, accounting for the inelastic scattering channels. $V_s(r)$ is the static potential, describing the interaction between the positron and the atomic charge density, and is repulsive in the case of positrons. We formulate this on a derivation of the Hartree–Fock atomic wavefunctions analogous to the work of Reid and Wadehra.[17] $V_p(r)$ is the polarization potential that accounts for the target electron cloud deformation during the collision and is therefore dependent on its atomic polarizability. We have shown in previous studies with oxygen (O) containing molecular targets how sensitive the low-energy elastic positron scattering is to the accuracy on the description of this term.[18,19] In that case, we used the sum of a dipole and a quadrupole potential calculated with the polarized-orbital method by determining the first-order corrections of the atomic orbitals due to a fixed charge field.[20] For O, the dipole and the quadrupole polarized-orbital potential of Ne (accurate against measurement[21]) were scaled according to the procedure described by Chiari et al.[19] A similar procedure is not available for the metallic atoms in which we are currently interested. Recently, for Be and Mg,[1] we used the energy dependent polarization potential proposed by Reid and Wadehra.[22] In the case of Zn and Cd, we have adopted a modified form of the polarization potential proposed by Jain.[23] Basically, it considers a positron correlation polarization potential (V_{corr}) for the inner region ($r < r_c$) and the standard asymptotic potential ($V_{asym} = -\alpha_d/2r^{-4}$) for $r > r_c$, where r_c is the so-called crossing radius and α_d is the atomic dipole polarizability (see Ref. [23] for details). The present modification provides a smoother join of both potentials for $r = r_c$ by imposing the condition $\frac{1}{V_p(r)} = \frac{1}{V_{corr}(r)} + \frac{1}{V_{asym}(r)}$ and includes a quadrupole polarization term as follows: $V_{asym}(r) = -\frac{\alpha_d}{r^4} - \frac{\alpha_q}{r^6}$, where α_q represents the atomic quadrupole polarizability. For these atoms, the quadrupole polarizabilities have been estimated by means of the Dalgarno–Lewis[24] approximation, $\alpha_q = \frac{2\alpha_d E_{rd}}{E_{rq}^2}$, where E_{rd} and E_{rq} are the threshold energies for the first resonant dipole and quadrupole transitions, respectively. $V_a(r)$ describes the "absorption" processes, i.e., the inelastic processes of discrete excitation, ionization, and positronium formation (Ps), and requires careful treatment. We use a scheme modified from that proposed by Reid and Wadehra,[22] assuming that the target electrons can be considered as a quasi-free electron cloud with which the incoming particles undergo binary collisions. The threshold energy is carefully designed to include Ps formation.

Our recent improvements to the treatment of Ps formation were outlined in detail previously.[11] In brief, we use an energy dependent threshold $\Delta(E)$ coinciding with the well-known Ps-formation threshold of $\Delta_p = I - 6.8$ eV (where I = ionization threshold) for lower energies (E < 3I) and the lowest optically allowed excitation transition energy Δ for higher impact energies (E ⩾ 3I) by assuming a smooth transition in threshold energy from low to high impact energy, which follows the expression

$$\Delta(E) = \Delta - (\Delta - \Delta_p) \Big/ \left[1 + \left(\frac{E}{3I} - 1 \right)^2 \right]. \tag{2}$$

TABLE 1. Relevant atomic data used in the present OP calculations

Atom	I (a.u.)	E_{rd} (a.u.)	E_{rq} (a.u.)	α_d (a.u.)	α_q[23] (a.u.)
Zn	0.3452	0.213	0.2845756	38.7	200
Cd	0.33051	0.19907	0.2698189	46	250

A similar procedure has been followed to extract the ionization cross section from the total inelastic cross section by using $\Delta = I$ as the threshold energy for the absorption potential.

The data required to calculate the above potentials and threshold energies (in atomic units) are presented in Table 1.

2.2. ROP details

The theoretical method used here to describe the elastic and inelastic scattering of positrons from zinc and cadmium atoms is based on the ROP method of Chen et al.,[25] hereafter referred to as I. This OP method is based on an approximate solution of the relativistic close-coupling equations and has been used previously to describe positron scattering from beryllium and magnesium (Blanco et al.[1]), hereafter referred to as II. Consequently, only a brief discussion of the overall method will be given here, and the reader is referred to I and II for details.

The scattering of the incident positrons, with wavenumber k, by zinc and cadmium atoms is described by the integral equation formulation of the partial wave Dirac–Fock scattering equations. In the ROP method, these equations can be written in the matrix form as

$$\begin{pmatrix} F_\kappa(r) \\ G_\kappa(r) \end{pmatrix} = \begin{pmatrix} v_1(kr) \\ v_2(kr) \end{pmatrix} + \frac{1}{k} \int_0^r dx\, G(r,x) \left[U(x) \begin{pmatrix} F_\kappa(x) \\ G_\kappa(x) \end{pmatrix} \right.$$
$$\left. - i\, U_{opt}(x) \begin{pmatrix} F_\kappa(x) \\ G_\kappa(x) \end{pmatrix} \right], \tag{3}$$

where the local potential $U(r)$ is given by the sum of the static and local polarization potentials, i.e.,

$$U(r) = U_{st}(r) + U_{pol}(r). \tag{4}$$

The static potentials were determined in the usual manner from the ground state Dirac–Fock orbitals of these atoms. Here, we used the procedure outlined by Bartschat et al.,[26,27] whereby the real part of the complex OP $U_{opt}(r)$ was replaced by the local polarization potential $U_{pol}(r)$ in Eq. (4). This potential was comprised of the sum of the first four multipole polarization potentials using the polarized-orbital method of McEachran et al.[20] Thus, in Eq. (3), the non-local potential $U_{opt}(r)$ denotes just the imaginary part of the OP, which, in turn, describes the absorption of the incident flux into the inelastic channels and thereby describes both excitation and ionization processes, including positronium formation. This potential is given by a sum and integration over the bound and continuum states of the atom (see Sec. 2.2.2 for details).

Finally, in Eq. (3), $F_\kappa(r)$ and $G_\kappa(r)$ are the large and small components of the complex scattering wavefunctions, while the functions $v_1(kr)$ and $v_2(kr)$ are the corresponding free particle wavefunctions and are given in terms of Riccati–Bessel functions. $G(r,x)$ is the free particle Green's function that can be expressed in the matrix form in terms of the Riccati–Bessel and Riccati–Neumann

functions (see Eq. 23 of I for details). The subscript κ on the scattering wavefunctions is the relativistic angular momentum quantum number of the incident positron. It is related to the corresponding orbital angular momentum quantum number l according to $\kappa = -l - 1$ when $j = l + 1/2$ (spin-up) and $\kappa = l$ when $j = l - 1/2$ (spin-down), where j is the total angular momentum quantum number of the incident positron.

The elastic and inelastic cross sections can be found once the complex partial wave phase shifts

$$\eta_l^{\pm}(k) = \delta_l^{\pm}(k) + i\,\gamma_l^{\pm}(k) \qquad (5)$$

have been determined from the large component of the complex scattering wavefunction [see Eqs. (5) and (6) of II]. The integrated elastic cross section is then given, in terms of these real and imaginary parts of the phase shifts, by

$$\sigma^{el}(k^2) = \frac{2\pi}{k^2} \sum_{l=0}^{\infty} \{(l+1)\exp(-2\gamma_l^+)\left[\cosh 2\gamma_l^+ - \cos 2\delta_l^+\right] \\ + l\exp(-2\gamma_l^-)\left[\cosh 2\gamma_l^- - \cos 2\delta_l^-\right]\}, \qquad (6)$$

while the total inelastic or absorption cross section is given by

$$\sigma^{inel}(k^2) = \frac{\pi}{k^2} \sum_{l=0}^{\infty} \{(l+1)\left[1-\exp(-4\gamma_l^+)\right] + l\left[1-\exp(-4\gamma_l^-)\right]\}. \qquad (7)$$

Here, the superscript + refers to "spin-up," while the superscript − refers to "spin-down."

2.2.1. Positronium formation

Here, positronium formation was simulated using the method given by McEachran and Stauffer,[28] which, in turn, is a modification of the method originally suggested by Reid and Wadehra.[17,29] In this method, the Ps-formation cross section is calculated by first determining the direct ionization cross section and then the comparable cross section when the ionization thresholds are reduced by 6.8 eV, the binding energy of ground state positronium. The Ps-formation cross section is then taken to be the difference between these two cross sections.

Any method for simulating rather than directly calculating Ps formation will contain one or more adjustable parameters. In the method of McEachran and Stauffer,[28] there is just one adjustable parameter that is chosen according to where the Ps-formation cross section effectively vanishes. As described in II, this adjustable parameter was chosen to be 200 + I eV. It should be noted that, in the method of McEachran and Stauffer, this adjustable parameter influences the asymptotic behavior of the Ps-formation cross section but has very little influence on its peak value.

2.2.2. The absorption potential

For zinc, the following eight bound excited states were included in $U_{opt}(r)$, namely, $np^{1,3}P^{\circ}$ with $n = 4$–7 in order to simulate excitation processes. Similarly, for cadmium, the corresponding states were included in $U_{opt}(r)$ with $n = 5$–8. Also included in $U_{opt}(r)$, for both zinc and cadmium, were all continuum states with orbital angular momentum given by $l_c = 0$, 1, and 2 in order to simulate ionization processes. The integration over the continuum states in the absorption potential was approximated by using Gauss–Legendre integration with 16 points. In a relativistic close-coupling expansion, it

is necessary to couple the total angular momentum of the electron in the excited state (bound or continuum) to the total angular momentum of the incident positron in order to obtain the total angular momentum J of the positron–atom system. This total angular momentum J is then conserved during the collision process. Under the above circumstances, this gave rise to a maximum of 24 excitation channels and 22 ionization channels in $U_{opt}(r)$ for both zinc and cadmium.

3. Data Comparison

In Fig. 1, we plot the available data[5,6] for positron scattering from Zn, along with our OP and ROP results for elastic scattering, positronium formation, the sum over discrete electronic-state excitation, and ionization scattering. There are several general observations we can make in relation to Fig. 1. First, as noted earlier, there are no experimental results against which we can compare the data from the theoretical computations. In addition, for positronium formation, discrete electronic-state excitation, and ionization, only the present OP and ROP results are now available. Considering first the elastic ICS at very low energies, then with the exception of our OP calculation, which is too high in magnitude due to the V_{pol} employed, the results from Mitroy et al.[6] and our ROP computation are in quite good accord. We explicitly investigated the dependence of the very low-energy elastic ICS, within our ROP framework, by varying the number of multipole terms retained in $U_{pol}(r)$. The resulting elastic ICS was found to be sensitive, in terms of both whether or not a plateau was observed in the ICS and in terms of the magnitude of the cross section at that plateau, to the number of multipoles retained in $U_{pol}(r)$. This result was also found for Cd (see below) and is entirely consistent with that found by Mitroy and co-workers,[6,7] who noted that the low-energy elastic ICS was very dependent on the form of the polarization potential adopted in the scattering calculations. In addition, we also note that the large elastic ICSs at very low energies, for both atoms, lead both atoms to have large magnitude scattering lengths.[30] As those respective magnitudes are larger than those for the mean radii of zinc and cadmium, it follows that the scattering cross sections will be greater than their geometric sizes. This enhancement, in each case, can be viewed[30] as arising from the existence of a virtual level for the positron projectile in both Zn and Cd. At energies above about 0.17 eV, the present ROP and OP results are in very good accord across the common energy range, while the calculation of Mitroy et al.[6] is somewhat higher in magnitude compared to both of them. Bromley[31] had suggested that his and his colleagues' approach might be accurate up to the positronium threshold energy (2.6 eV for zinc), but the results in Fig. 1 indicate that it may only be accurate below ~0.2 eV. The theoretical elastic ICS results from Szmytkowski[5] are generally lower in magnitude than those from all the other calculations, and the shape of the ICS as a function of E_0 does not appear to be physical. As a consequence, we do not consider it in our further deliberations. For the positronium formation [Fig. 1(b)], sum over discrete electronic-state excitation [Fig. 1(c)], and ionization [Fig. 1(d)] ICSs, our OP and ROP computations are in reasonable qualitative accord although some differences in the magnitude of the cross sections are noted. Of particular interest in Fig. 1(c) is a near-threshold structure that can be ascribed to the excitation of the 4^3P state of Zn. In a non-relativistic calculation, excitation of this state could only occur via electron exchange, which is not available in
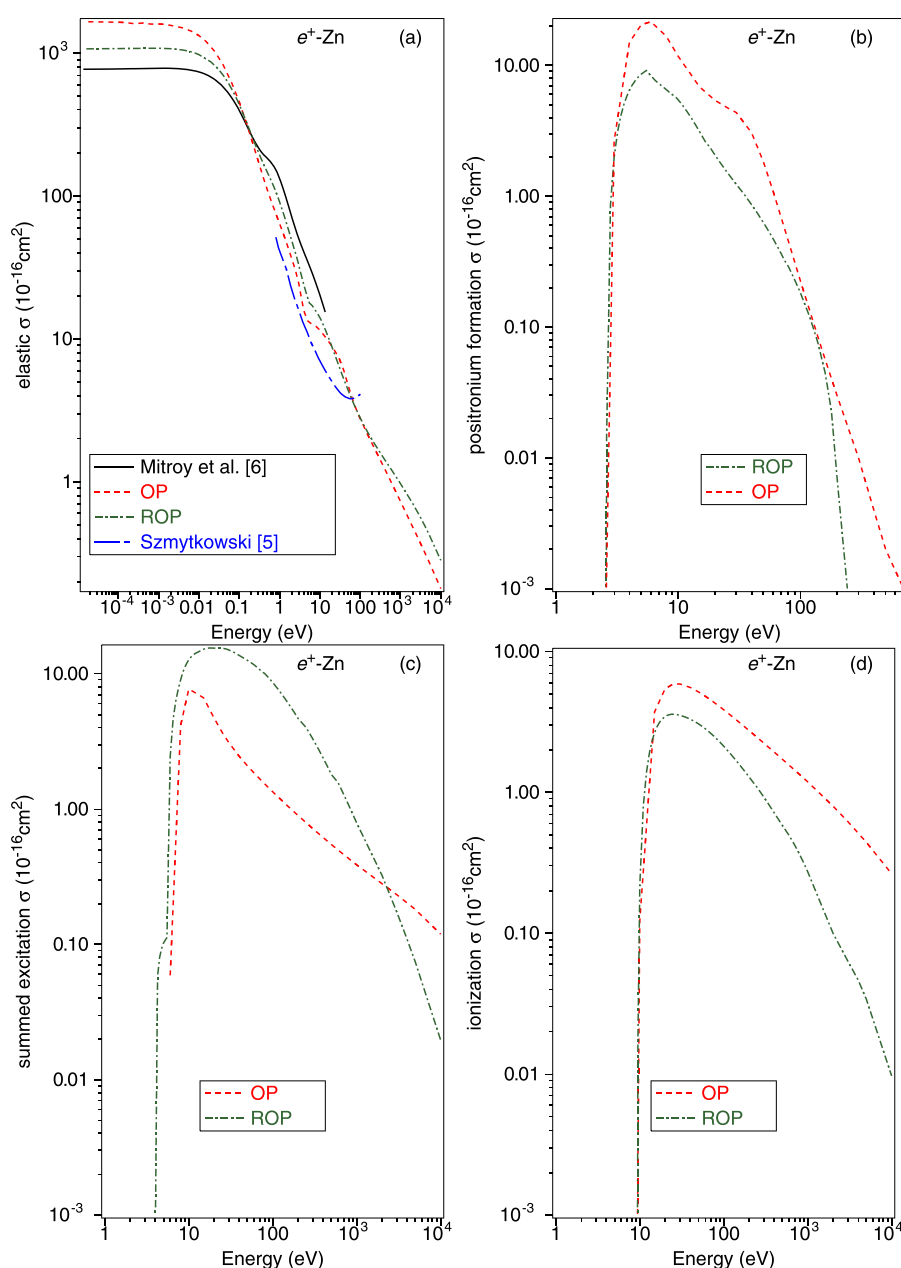
FIG. 1. The presently available cross sections (10^{-16} cm^2) for positron scattering from zinc. (a) Elastic scattering, (b) positronium formation, (c) summed discrete electronic-state excitation, and (d) total ionization. See also the legend in the figure.

positron scattering, and so one might anticipate its cross section to be zero. However, in a relativistic framework (such as in our ROP results), this is not the case due to configuration mixing, and although the interaction is quite weak, it will be non-zero, as shown in Fig. 1(c).

A similar comparison to that just given, but now for positron–Cd scattering, is made for the same scattering processes in Fig. 2. Again, we notice that there are no experimental data to compare against, and similar to what we found in Zn, only our new OP and ROP results are

available for positronium formation, the sum over discrete electronic states, and ionization. Considering Fig. 2(a) in more detail, for the elastic ICS, we notice very good qualitative agreement between the OP, ROP, and Bromley and Mitroy[7] computations below about 0.15 eV, with all three datasets indicating that the elastic cross section plateaus in magnitude below about 0.01 eV in energy. Above 0.15 eV, the present OP and ROP computations remain in good accord across their common energy range, while the elastic ICS of Bromley and
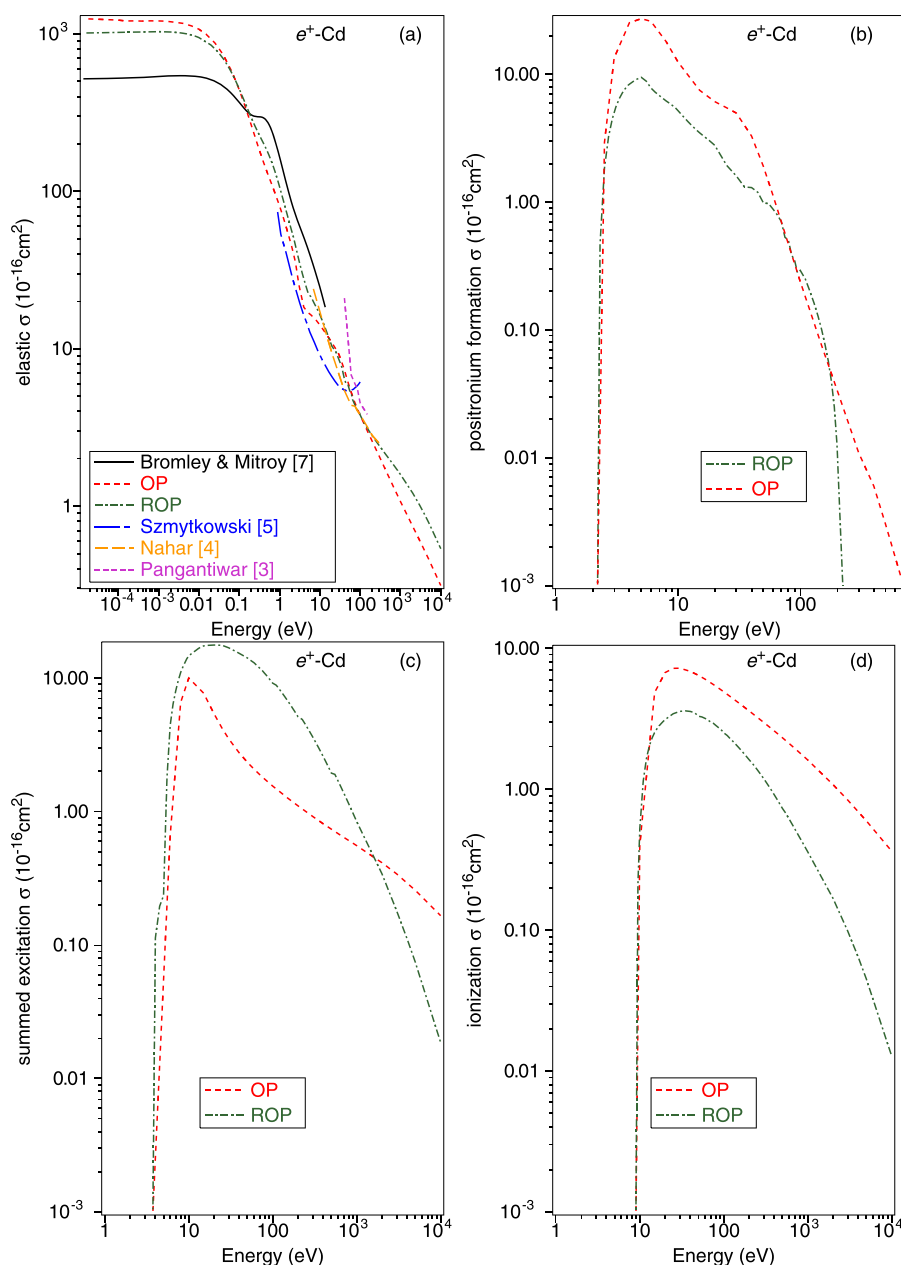
FIG. 2. The presently available cross sections (10^{-16} cm^2) for positron scattering from cadmium. (a) Elastic scattering, (b) positronium formation, (c) summed discrete electronic-state excitation, and (d) total ionization. See also the legend in the figure.

Mitroy is somewhat higher in magnitude. In the case of Cd, the threshold energy for positronium formation (E_{Ps}) is about 2.2 eV. Thus, the expectation of Bromley[31] that the CDU approach might be expected to be valid up to E_{Ps} is again shown to be a little optimistic. The results in Fig. 2(a) indeed suggest that its range of validity is likely to be for $E_0 \lesssim 0.2$ eV. We note that both our OP and ROP calculations, in Cd and Zn, exhibit a shoulder in their elastic ICS in the energy range ~5 to 7 eV [see Figs. 1(a) and 2(a)]. We believe this shoulder arises due

to a flux competition effect between the elastic channel and the 4^1P optically allowed state of Zn and 5^1P optically allowed state in Cd, respectively, which open in that ~5 to 7 eV energy window. At higher energies (E_0 = 40–150 eV), the elastic ICS of Pangantiwar and Srivastava[3] is also higher in magnitude when compared to the present results, while, similar to what we described above for Zn, the Szmytkowski[5] calculation is lower in magnitude over the common energy range and its shape, as a function of energy, does not look very

TABLE 2. Present recommended cross sections (10^{-16} cm^2) for positron scattering from Zn

Energy (eV)	Elastic scattering	Summed excitation	Ionization	Positronium formation	TCS
0.1361×10^{-4}	919.2				919.2
0.1000×10^{-2}	930.7				930.7
0.2000×10^{-1}	771.3				771.3
0.3000×10^{-1}	699.5				699.5
0.4000×10^{-1}	638.9				638.9
0.5000×10^{-1}	587.3				587.3
0.6000×10^{-1}	543.0				543.0
0.7000×10^{-1}	504.7				504.7
0.8000×10^{-1}	471.4				471.4
0.1000	416.3				416.3
0.1500	323.4				323.4
0.2000	260.3				260.3
0.2500	220.7				220.7
0.3000	187.4				187.4
0.3500	167.7				167.7
0.4000	150.3				150.3
0.5000	128.0				128.0
0.6000	113.8				113.8
0.7000	101.1				101.1
0.8000	92.60				92.60
1.000	77.61				77.61
1.250	64.75				64.75
1.500	55.33				55.33
1.750	48.51				48.51
2.000	42.70				42.70
2.250	38.50				38.50
2.500	34.81				34.81
2.591	33.67			0.0000	33.67
2.600	33.56			0.3586×10^{-1}	33.59
2.800	31.00			1.107	32.11
3.000	28.57			2.319	30.89
3.200	26.55			4.113	30.67
3.400	24.69			5.857	30.55
3.800	21.35			9.168	30.52
4.006	19.81	0.0000		10.77	30.58
4.500	17.92	0.8030×10^{-1}		12.74	30.75
5.000	16.34	0.1024		14.54	30.99
5.500	15.44	0.1123		15.11	30.66
6.000	15.13	2.428		15.00	32.55
6.500	14.87	4.581		14.06	33.51
7.000	14.53	6.286		13.23	34.04
8.500	13.63	10.25		10.89	34.77
9.391	13.14	11.85	0.0000	9.574	34.56
9.500	13.08	12.02	0.1967×10^{-1}	9.416	34.53
10.00	12.80	12.67	0.1694	8.655	34.30
11.00	12.28	13.64	0.8169	7.864	34.61
12.00	11.77	14.15	1.469	7.104	34.49
13.00	11.29	14.50	2.085	6.372	34.25
14.00	10.84	14.86	2.656	5.668	34.03
15.00	10.42	15.18	3.184	4.991	33.77
16.00	10.06	15.38	3.486	4.694	33.62
17.00	9.712	15.47	3.757	4.421	33.36

TABLE 2. (*Continued.*)

Energy (eV)	Elastic scattering	Summed excitation	Ionization	Positronium formation	TCS
18.00	9.408	15.49	4.003	4.209	33.12
20.00	8.811	15.46	4.443	3.755	32.47
22.00	8.334	15.45	4.578	3.498	31.86
25.00	7.702	15.43	4.727	3.165	31.02
30.00	6.878	15.00	4.699	2.799	29.38
35.00	6.162	14.32	4.565	2.370	27.41
40.00	5.534	13.64	4.426	1.962	25.56
45.00	5.034	13.06	4.270	1.590	23.96
50.00	4.577	12.56	4.114	1.231	22.48
60.00	3.948	11.63	3.825	0.7832	20.18
70.00	3.520	10.71	3.572	0.5231	18.33
75.00	3.361	10.27	3.460	0.4437	17.53
80.00	3.210	10.06	3.352	0.3715	16.99
90.00	2.987	9.302	3.166	0.2853	15.74
100.0	2.785	8.617	2.990	0.2060	14.60
120.0	2.529	7.464	2.731	0.1477	12.87
140.0	2.310	6.546	2.497	0.8940×10^{-1}	11.44
150.0	2.225	6.175	2.402	0.6025×10^{-1}	10.86
160.0	2.141	5.804	2.307	0.5351×10^{-1}	10.31
180.0	2.014	5.192	2.157	0.4005×10^{-1}	9.403
200.0	1.898	4.680	2.017	0.2658×10^{-1}	8.621
250.0	1.709	4.001	1.787	0.1772×10^{-1}	7.514
300.0	1.546	3.301	1.581	0.8860×10^{-2}	6.437
350.0	1.438	2.776	1.444	0.6202×10^{-2}	5.665
400.0	1.340	2.372	1.321	0.3544×10^{-2}	5.037
450.0	1.268	2.053	1.231	0.2658×10^{-2}	4.555
500.0	1.201	1.798	1.149	0.1772×10^{-2}	4.149
600.0	1.103	1.569	1.036	0.1329×10^{-2}	3.710
674.3	1.039	1.357	0.9574	0.1000×10^{-2}	3.354
700.0	1.016	1.283	0.9301		3.230
800.0	0.9562	1.073	0.8587		2.888
900.0	0.9012	0.9136	0.7922		2.607
1000	0.8499	0.7889	0.7300		2.369
2000	0.5954	0.3242	0.4496		1.369
3000	0.4786	0.1735	0.3422		0.9943
4000	0.4115	0.1083	0.2889		0.8088
5000	0.3565	0.7370×10^{-1}	0.2379		0.6682
10 000	0.2305	0.1960×10^{-1}	0.1368		0.3870

physical. On the other hand, the elastic-ICS computation of Nahar[4] is in very good accord with our present calculations across the energy region where they overlap [see Fig. 2(a)]. In Fig. 2(b), we plot the available positronium formation cross sections; in Fig. 2(c), we show the summed discrete electronic-state excitation cross sections; and in Fig. 2(d), we plot the TICSs for positron–Cd scattering. In each case, similar to that found above for Zn, we find good qualitative convergence between our OP and ROP calculations. The positronium formation cross section [see Fig. 2(b)] has a form very similar to those of other atomic systems where such data are available.[2] Namely, the cross section rises very steeply in magnitude from its threshold energy until a peak magnitude is reached at about two to three times the value of E_{Ps}. A similar behavior was also seen in both our OP and ROP calculations for positron–Zn scattering [see Fig. 1(b)]. Here, we also

highlight a near-threshold structure in the ROP in Fig. 2(c), whose origin is due to excitation of the optically forbidden 5^3P state and which occurs due to configuration mixing within our relativistic framework.

4. Recommended Data

Based largely on the discussion in Sec. III, here, we now construct our recommended cross section datasets for positron–Zn (see Table 2 and Fig. 3, upper pane) and positron–Cd (see Table 3 and Fig. 3, lower pane) scattering in the gas phase. In many instances, where there were only two calculations available and there was no *a priori* reason for us to prefer one over the other, we followed the method of Itikawa[32] to determine our recommended cross sections. In this approach, a
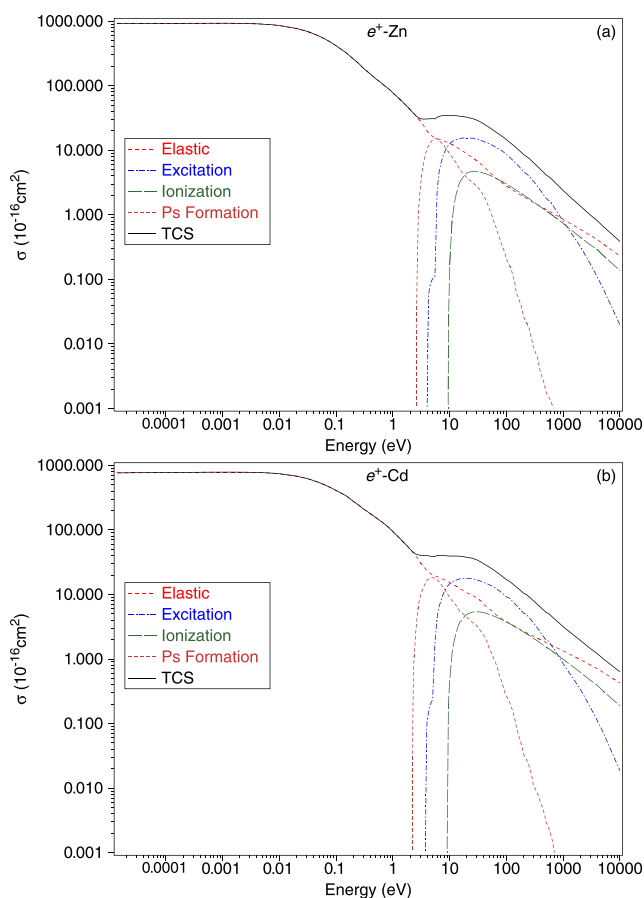
FIG. 3. Present recommended cross sections (10^{-16} cm²) for positron scattering from (a) Zn and (b) Cd. See also the legend in figures and Tables 2 and 3.

simple average of the available cross section data is made, with uncertainty limits chosen to reflect the variance between those data. Note that we have successfully applied this method in some of our earlier electron–atom[16,33–35] and positron–atom[1] reviews.

For positron–zinc scattering, we form the recommended elastic ICS by taking an average of the results of Mitroy *et al.*[6] and present ROP results up to 0.1694 eV and then mapping onto that an average of our ROP and OP calculations (scaling factor = 1.0001 to ensure continuity) to extend the results up to 10 000 eV. The resulting recommended elastic cross sections can be found in Table 2 and can be viewed in Fig. 3(a). Given the level of accord between the various calculations, a conservative uncertainty estimate of ±30% up to 0.1694 eV and ±20% thereafter on the uncertainty of the elastic ICS seems reasonable. In the case of positronium formation, we form the recommended cross sections by simply taking an average of the present ROP and OP results. Here, we ascribe an uncertainty of ±25% to the resulting data, which can also be found in Table 2 and in Fig. 3(a). For the summed discrete electronic-state excitation ICSs, Fig. 1(c) clearly shows that our non-ROP result trends toward an incorrect threshold energy. As a consequence, here, the recommended ICS is formed only from our ROP calculation with an

uncertainty of ±30% assigned to it [again see Table 2 and Fig. 3(a)]. With respect to the total ionization cross section, the near-threshold behavior and threshold energies of both our OP and ROP computations are highly consistent. Therefore, our recommended TICS is formed from a simple average of our ROP and OP calculations with the result of this process being found in Table 2 and Fig. 3(a). In this case, an uncertainty of ±25% is assigned to the TICS. Finally, by adding at each E_0 the elastic ICS, Ps-formation ICS, summed discrete electronic-state excitation ICS, and TICS, the grand TCS is formed for positron–Zn scattering. These data are found in Table 2 and Fig. 3(a), with an uncertainty of ±30% ascribed to $E_0 \leqslant 0.1694$ eV and an uncertainty of ±25% assigned at all higher energies up to 10 000 eV.

Let us now consider Cd. Here, the recommended elastic ICS is found by taking an average of the results of Bromley and Mitroy[7] and our ROP results up to 0.1539 eV and then mapping onto that an average of our OP and ROP computations (scaling factor = 1.00001) to ensure continuity to extend the results up to 10 000 eV. The resulting recommended elastic ICSs can be found in Table 3 and can be seen in Fig. 3(b). Given the level of agreement between the various calculations, a conservative uncertainty estimate of ±30% up to 0.1539 eV and ±20% thereafter up to 10 000 eV on the elastic ICS seems justifiable. For positronium formation, we construct our recommended cross sections by simply taking an average of the current OP and ROP results. Here, we assign an uncertainty of ±25% on the resulting data, which can also be found in Table 3 and in Fig. 3(b). In the case of the summed discrete electronic-state excitation ICSs, Fig. 2(c) shows that the non-ROP calculation does not account for excitation of the optically forbidden 5^3P state of Cd, and so as a consequence, we form its recommended ICS from our ROP computation alone. These data are also listed in Table 3 and plotted in Fig. 3(b), with an uncertainty of ±30% being ascribed to them. The positron–Cd TICS is also constructed from an average of our ROP and OP results [see Table 3 and Fig. 3(b)], with an estimated uncertainty of ±25% being assigned to it. Finally, again by adding together at each E_0 the elastic ICS, Ps-formation ICS, summed discrete electronic-state ICSs, and TICS, the TCS for positron–Cd scattering is formed. These data are found in Table 3 and Fig. 3(b), with an uncertainty of ±30% ascribed to $E_0 \leqslant 0.1539$ eV and an uncertainty of ±25% for all higher energies up to 10 000 eV.

5. Transport Simulations

In this section, we simulate the transport of positron swarms in gaseous Zn and Cd using the recommended positron–Zn and positron–Cd cross section databases shown in Tables 2 and 3. For comparison, we also simulate electron transport in gaseous Zn using the recommended set published by McEachran *et al.*[16] In all the calculations, we assume isotropic scattering for the electronic-state excitation and ionization processes, while we account for the anisotropic nature of elastic scattering through the use of momentum transfer cross sections (MTCSs). We determine a suitable elastic MTCS in each case by scaling the recommended elastic ICS by using the form of the corresponding ROP differential cross section. To perform the swarm transport calculations, we apply a well-benchmarked multi-term solution of Boltzmann's equation[13,36,37] across a range of reduced electric fields, E/n_0, varying from 10^{-2} Td to 10^3 Td, where 1 Td = 1 Townsend = 10^{-21} V m² and n_0 is the neutral

TABLE 3. Present recommended cross sections (10^{-16} cm^2) for positron scattering from Cd

| Energy (eV)	Elastic scattering	Summed excitation	Ionization	Positronium formation	TCS
0.1361×10^{-4}	765.8				765.8
0.1000×10^{-2}	785.1				785.1
0.5000×10^{-2}	771.5				771.5
0.2000×10^{-1}	680.9				680.9
0.4000×10^{-1}	581.2				581.2
0.6000×10^{-1}	506.9				506.9
0.8000×10^{-1}	450.8				450.8
0.1000	407.7				407.7
0.1500	337.4				337.4
0.2000	277.6				277.6
0.2500	241.9				241.9
0.3000	211.9				211.9
0.4000	177.5				177.5
0.5000	154.9				154.9
0.7000	124.0				124.0
0.8000	113.0				113.0
1.000	93.97				93.97
1.250	77.42				77.42
1.500	65.62				65.62
1.750	57.37				57.37
2.000	50.39				50.39
2.196	46.26			0.0000	46.26
2.196	46.25			0.1577×10^{-2}	46.26
2.300	44.07			0.7352	44.81
2.500	40.03			2.383	42.41
2.700	36.32			5.182	41.50
2.900	32.90			7.902	40.80
3.100	30.29			10.07	40.36
3.300	28.45			11.70	40.15
3.734	24.98	0.0000		14.97	39.95
4.000	23.08	0.1130		16.83	40.02
5.000	20.00	0.2341		18.34	38.57
5.500	19.32	1.800		17.70	38.82
6.000	18.90	4.402		16.88	40.18
8.000	16.87	11.01		12.08	39.97
8.996	16.08	13.06	0.0000	10.47	39.61
9.500	15.68	14.02	0.2061	9.655	39.56
10.00	15.30	14.65	0.4630	8.822	39.24
11.00	14.63	15.42	1.222	8.076	39.36
12.00	14.02	16.03	1.919	7.378	39.35
13.00	13.46	16.65	2.554	6.719	39.39
14.00	12.93	17.14	3.139	6.094	39.30
15.00	12.43	17.42	3.691	5.494	39.04
18.00	11.28	17.63	4.459	4.846	38.22
20.00	10.63	17.70	4.931	4.439	37.69
25.00	9.750	17.60	5.332	3.699	36.38
30.00	8.826	16.85	5.406	3.284	34.37
35.00	7.971	16.02	5.330	2.719	32.04
40.00	6.994	15.32	5.225	2.289	29.82
45.00	6.359	14.69	5.077	1.890	28.02
50.00	6.001	14.14	4.873	1.439	26.45
55.00	5.556	13.53	4.753	1.241	25.08

TABLE 3. (Continued.)

Energy (eV)	Elastic scattering	Summed excitation	Ionization	Positronium formation	TCS
60.00	5.236	13.01	4.617	0.9988	23.86
65.00	4.875	12.40	4.486	0.8515	22.62
75.00	4.446	11.40	4.250	0.5580	20.65
80.00	4.280	10.86	4.129	0.4868	19.76
85.00	4.139	10.42	4.027	0.3984	18.98
90.00	4.005	9.965	3.926	0.3516	18.25
95.00	3.936	9.534	3.829	0.2879	17.59
100.0	3.786	9.160	3.720	0.2655	16.93
110.0	3.613	8.852	3.586	0.2282	16.28
120.0	3.466	8.255	3.440	0.1871	15.35
130.0	3.324	7.705	3.308	0.1508	14.49
140.0	3.195	7.221	3.177	0.1177	13.71
150.0	3.072	6.786	3.051	0.8740×10^{-1}	13.00
160.0	2.988	6.394	2.958	0.7120×10^{-1}	12.41
170.0	2.908	6.035	2.869	0.5755×10^{-1}	11.87
200.0	2.686	5.135	2.616	0.3339×10^{-1}	10.47
225.0	2.563	4.900	2.475	0.2774×10^{-1}	9.965
250.0	2.448	4.401	2.338	0.2210×10^{-1}	9.209
275.0	2.342	3.977	2.208	0.1645×10^{-1}	8.543
300.0	2.240	3.614	2.085	0.1080×10^{-1}	7.949
325.0	2.169	3.300	1.996	0.9575×10^{-2}	7.475
350.0	2.102	3.026	1.912	0.8348×10^{-2}	7.049
400.0	1.975	2.576	1.754	0.5892×10^{-2}	6.311
450.0	1.880	2.223	1.637	0.4419×10^{-2}	5.744
500.0	1.792	1.941	1.528	0.2946×10^{-2}	5.263
550.0	1.727	1.899	1.453	0.2455×10^{-2}	5.081
600.0	1.665	1.696	1.378	0.1964×10^{-2}	4.742
650.0	1.606	1.527	1.308	0.1473×10^{-2}	4.442
698.2	1.552	1.388	1.243	0.1000×10^{-2}	4.184
700.0	1.550	1.383	1.241		4.173
800.0	1.471	1.152	1.150		3.773
900.0	1.398	0.9779	1.066		3.442
1000	1.329	0.8421	0.9882		3.159
2000	0.9792	0.3415	0.6248		1.945
3000	0.8090	0.1797	0.4687		1.457
4000	0.7074	0.1105	0.3911		1.209
5000	0.6239	0.7410×10^{-1}	0.3210		1.019
10 000	0.4248	0.1860×10^{-1}	0.1884		0.6318

number density. In each case, we consider a vapor temperature of 750 K, which was chosen to be consistent with our earlier transport simulations of electrons and positrons in gaseous Be and Mg[1] and electrons in gaseous Zn.[16] We confirm the results of McEachran *et al.*[16] and find that the two-term approximation (TTA)[36,37] is suitably accurate (within a few percent) for electron–Zn transport, with the exception of the diffusion calculations above ~100 Td, which can be in error by up to 43% at 1000 Td. In contrast, we find the TTA to be highly inadequate for describing positron–Zn and positron–Cd transport, generally exceeding a few percent error by only ~25 Td, regardless of the transport coefficient under consideration. The transverse diffusion coefficients are those worst affected by the TTA, increasing in error by up to 2000% by 400 Td, before becoming numerically unstable at even higher E/n_0. Given such large errors, it is

unsurprising that the TTA can also result in negative diffusion coefficients, as shown in Fig. 4 for the case of the bulk (center-of-mass) longitudinal diffusion of a positron swarm in Zn vapor. We conclude that to determine all of the considered transport coefficients to within an accuracy of 1%, at least a four-term approximation is required in the case of electron transport and at least a ten-term approximation is required in the cases of positron transport. Figure 5 presents our electron and positron transport calculations, containing plots of mean electron/positron energies, $\bar{\varepsilon}$; process rate coefficients, k; drift velocities, W; reduced mobilities, $n_0\mu$; reduced longitudinal diffusion coefficients, $n_0 D_L$; and reduced transverse diffusion coefficients, $n_0 D_T$. In what follows, we discuss positron transport in gaseous Zn and Cd, before comparing electron and positron transport in gaseous Zn.
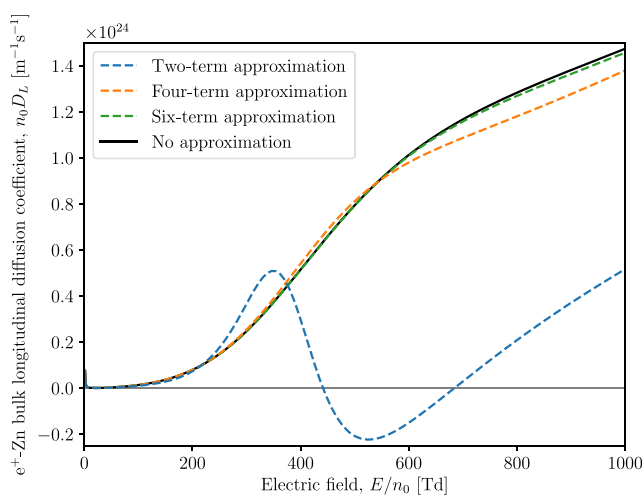
FIG. 4. The TTA can be inaccurate to the extent of producing negative diffusion coefficients, as is shown here for the bulk (center-of-mass) longitudinal diffusion of a positron swarm in Zn vapor. For the specific coefficients plotted here, at least an eight-term approximation is necessary to ensure an accuracy of within 1%. See also the legend for further details.

5.1. Positron transport in gaseous Zn and Cd

Figure 5 exhibits similar transport coefficients for positrons in both Zn and Cd vapors, as is expected given the similarities between the positron–Zn and positron–Cd recommended cross section sets (see Fig. 3). Figure 5(a) shows that, in each case, the positrons begin in thermal equilibrium with the background vapor of thermal energy $\frac{3}{2}k_B T \approx 97$ meV, before monotonically increasing in mean energy with increasing E/n_0. Due to the larger elastic MTCS for positron–Zn scattering at low energies, positrons experience additional elastic cooling at low E/n_0 in Zn compared to Cd, resulting in the mean positron energy in Zn departing from thermal equilibrium later than in Cd. However, by ~3.3 Td, the mean positron energy in Zn catches up to and subsequently exceeds that for Cd due to the larger amount of Ps-formation cooling in Cd stemming from the smaller threshold energy and larger peak magnitude of the positron–Cd Ps-formation cross section. Figure 5(b) shows plots of the rate coefficients for elastic momentum transfer, excitation, ionization, and Ps formation. Elastic momentum transfer rate coefficients for positron transport in Zn and Cd both decrease monotonically with increasing E/n_0, which is expected in each case given the corresponding monotonic decreases in each elastic MTCS with increasing energy. Excitation, ionization, and Ps-formation rate coefficients all increase monotonically with increasing E/n_0 while generally doing so in the order of their corresponding cross section threshold energies. The only exceptions here are the excitation and ionization rate coefficients for positron–Cd scattering, which rise later than their Zn counterparts despite having smaller corresponding threshold energies. This is due to the aforementioned smaller mean positron energy in Cd compared to Zn beyond ~3.3 Td. Figures 5(c) and 5(d) give plots of positron drift velocities and reduced mobilities, respectively. Positron mobilities remain constant up to ~1 Td, resulting in linearly increasing drift velocities in this lower E/n_0 regime. From 1 Td to 3 Td, positron flux

mobilities increase by roughly fourfold before remaining constant, for the most part, up to 1000 Td. The flux drift velocities transition accordingly between these separate linear regimes (<1 Td and >3 Td). The bulk drift velocities, on the other hand, coincide with the flux drift velocities only up until ~1 Td, after which they exhibit significant NDC and decrease to a minimum near ~40 Td that is three orders of magnitude smaller than their flux counterparts at this E/n_0. NDC arises here due to the preferential loss of positrons toward the front of the swarm due to Ps formation, thus shifting the swarm's center of mass backward. At higher E/n_0, the bulk drift velocities and mobilities for the positron swarms increase, almost matching the magnitude of their flux counterparts by 1000 Td. Figure 5(e) shows plots of the reduced longitudinal diffusion coefficients, which all follow similar qualitative trends to the reduced mobility plots in Fig. 5(d) due to the same nonconservative effects that were highlighted above. Finally, Fig. 5(f) gives plots of the reduced transverse diffusion coefficients, which are somewhat qualitatively similar to their longitudinal counterparts in Fig. 5(e), although with a much smaller difference between flux and bulk transverse diffusion from ~1 Td onward. We attribute the discrepancy that is present here to the preferential formation of Ps around the energetic edges of the swarm, thus contracting the swarm transversely.

5.2. Comparison of electron and positron transport in gaseous Zn

Figure 5 also shows significant differences between electron and positron transport coefficients in gaseous Zn. As the excitation and ionization cross sections are fairly similar between electron–Zn and positron–Zn scattering, these differences are expected to be primarily due to the differences in the elastic MTCS, as well as the absence/presence of the Ps-formation channel. Figure 5(a) shows that, as with the mean positron energy in Zn, the mean electron energy in Zn also increases monotonically from thermal equilibrium. However, the departure from the thermal equilibrium of positrons in Zn is seen to occur at a larger E/n_0 than for electrons due to the cooling effect of Ps formation. At higher E/n_0, near 5 Td, both electron and positron mean energies in Zn experience a plateau that persists up to ~150 Td. While this was attributed to Ps formation in the case of positron transport, we attribute the mean electron energy plateau instead to the opening of the electron–Zn inelastic excitation channels.[16] Figure 5(b) shows all the electron–Zn rate coefficients (i.e., for elastic momentum transfer, excitation, and ionization). The elastic momentum transfer rate coefficient for electron–Zn scattering at low E/n_0 (<10^{-2} Td) begins an order of magnitude smaller than its positron counterpart due to its corresponding two orders of magnitude smaller elastic MTCS at low energies (<0.1 eV). As the electron–Zn elastic MTCS increases in magnitude with respect to energy to a maximum near 0.6 eV, the electron–Zn elastic momentum transfer rate coefficient also increases accordingly with increasing E/n_0, before exceeding that for positron–Zn collisions by ~3 Td and then remaining roughly constant up to 1000 Td. The excitation and ionization rate coefficients for electron–Zn scattering both increase monotonically with increasing E/n_0 and are seen to do so earlier than their positron counterparts due to the absence of Ps-formation cooling for electrons. Figures 5(c) and 5(d) give plots of electron drift velocities in Zn and corresponding reduced electron mobilities, respectively. The electron mobilities are initially constant at low E/n_0
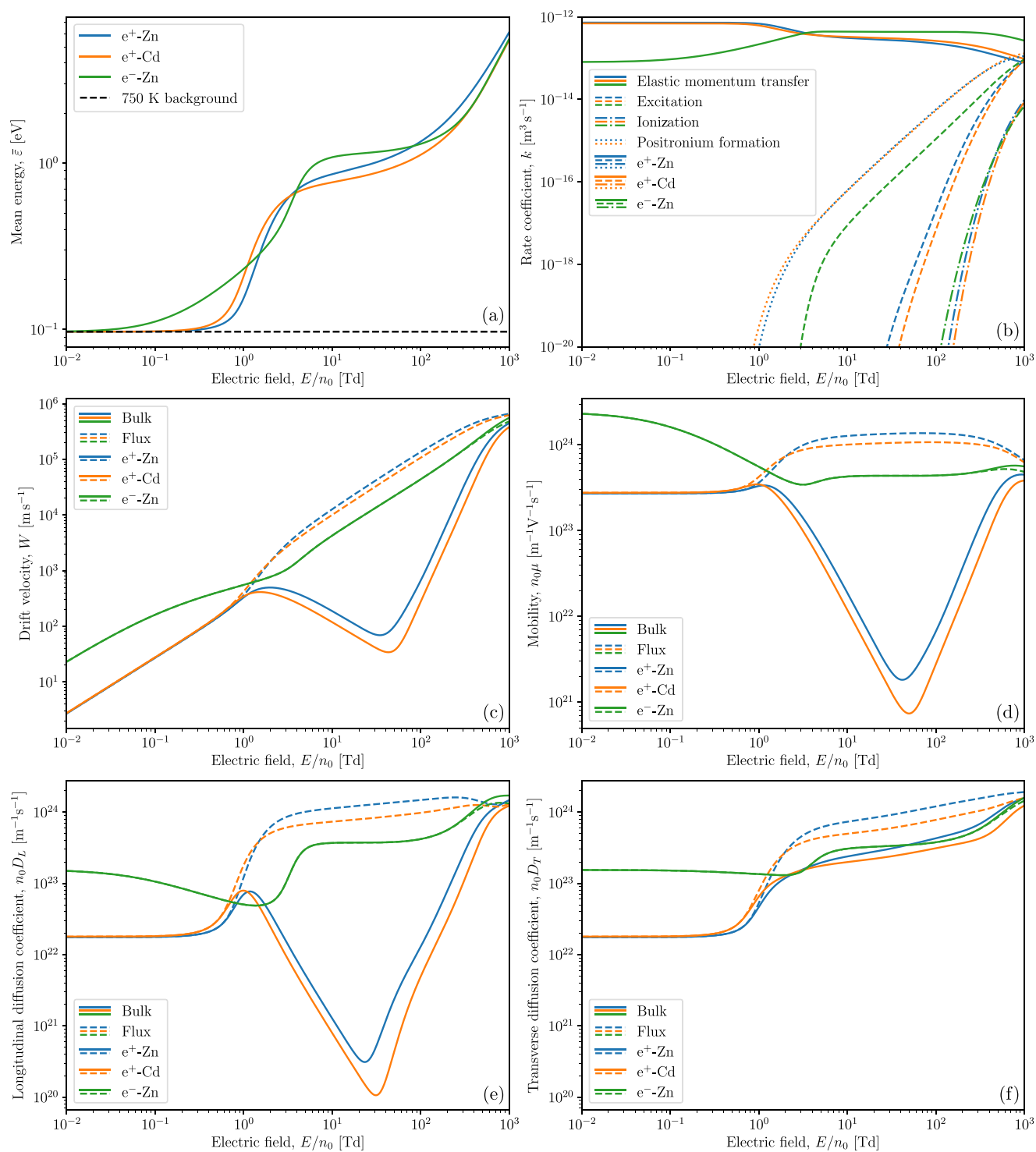
FIG. 5. Calculated mean electron/positron energies (a), rate coefficients (b), drift velocities (c), reduced mobilities (d), reduced longitudinal diffusion coefficients (e), and reduced transverse diffusion coefficients (f) for positrons in Zn vapor (blue), positrons in Cd vapor (orange), and electrons in Zn vapor (green). All vapors are of temperature $T = 750$ K, with a corresponding thermal energy of $\frac{3}{2}k_B T \approx 97$ meV. All calculations are performed over a range of reduced electric fields, E/n_0, from 10^{-2} Td to 10^3 Td. See also the legends for further details.

($<10^{-2}$ Td), with a value that is an order of magnitude larger than that for positrons in the same regime due to the much smaller elastic MTCS for electron–Zn scattering compared to positron–Zn scattering at low energies (<0.1 eV). At higher E/n_0, the electron mobilities decrease primarily due to the elastic MTCS increasing with energy, ultimately decreasing by an order of magnitude by 2 Td, after which they remain roughly constant up to 1000 Td. The electron drift velocities, of course, vary accordingly. At high E/n_0 (>400 Td), the preferential production of electrons due to ionization at the front of the swarm shifts the center of mass forward, thus causing the bulk drift velocity and bulk mobility to exceed their flux counterparts. This macroscopic phenomenon does not affect the positron–Zn bulk transport coefficients as ionization is a conservative process in the case of positron transport. Finally, Figs. 5(e) and 5(f) show plots of the reduced longitudinal diffusion coefficients and reduced transverse diffusion coefficients, respectively, for electron collisions in Zn. As for the drift velocities, these coefficients also begin an order of magnitude larger than their positron counterparts, which is due once again to the smaller elastic MTCS for electron–Zn scattering at low energies (<0.1 eV). As expected, we again see nonconservative effects at high E/n_0 (>400 Td), with the bulk diffusion exceeding the flux diffusion due to the preferential production of electrons due to ionization around the energetic edges of the swarm, thus causing the electron swarm to expand both longitudinally and transversely.

6. Conclusions

We have reported on results from our OP and ROP methodologies for positron scattering from zinc and cadmium. Together with the somewhat limited results from previous work,[3–7] we were able to use our new computations to construct recommended ICS databases for positron–Zn and positron–Cd scattering. A clear need for experimental measurements in both collision systems was also identified. We also presented a comparative study of positron transport in Zn and Cd gases at 750 K and have shown that the relevant transport coefficients are typically quite similar for the two metal vapors. Note that the transport coefficients we determined are in principle sensitive to the temperature of the background gas under consideration. For the specific case of positron transport in Cd, and for temperatures of 375, 750, and 1500 K, the values of the mean energies at each T were found to only coincide above 5 Td and the drift velocities only coincided above about 2 Td, while the diffusion coefficients were more sensitive to temperature and only coincided beyond 50 Td. The similarities we observed represent the macroscopic manifestation of similarities in their common positron scattering cross sections. We therefore also highlight that experimental transport measurements for both these species are highly desirable; in particular, they might represent the best opportunity to validate the very low-energy cross sections ($\lesssim 0.2$ eV). This demonstrates the importance of an accurate and complete set of cross sections for positrons (and electrons[38]) when modeling their transport in metal vapors, and indeed, the suggested transport measurements also represent an independent method of testing the accuracy and self-consistency of the cross section sets. Finally, in the case of gaseous Zn, we compared the transport behavior of both electrons and positrons at 750 K. Here, some quite significant differences were found, reflecting, at least in part, the differences in the fundamental nature of the interactions available to electrons and positrons, e.g., exchange in electrons and positronium formation with positrons, as well as the polarization interaction being attractive for both electrons and positrons and the static interaction being attractive for electrons and repulsive for positrons.

7. Supplementary Material

Please see the supplementary materials for Excel format files of each of the tables of this paper.

Data Availability

The data that support the findings of this study are available from the corresponding author upon reasonable request.

8. References

[1] F. Blanco, G. García, R. P. McEachran, P. W. Stokes, R. D. White, and M. J. Brunger, J. Phys. Chem. Ref. Data **48**, 033103 (2019).

[2] K. Ratnavelu, M. J. Brunger, and S. J. Buckman, J. Phys. Chem. Ref. Data **48**, 023102 (2019).

[3] A. W. Pangantiwar and R. Srivastava, Phys. Rev. A **40**, 2346 (1989).

[4] S. N. Nahar, Phys. Rev. A **43**, 2223 (1991).

[5] R. Szmytkowski, Acta Phys. Pol., A **84**, 1035 (1993).

[6] J. Mitroy, J. Y. Zhang, M. W. J. Bromley, and S. I. Young, Phys. Rev. A **78**, 012715 (2008).

[7] M. W. J. Bromley and J. Mitroy, Phys. Rev. A **81**, 052708 (2010).

[8] H. Tanaka, M. J. Brunger, L. Campbell, H. Kato, M. Hoshino, and A. R. P. Rau, Rev. Mod. Phys. **88**, 025004 (2016).

[9] W. J. Tattersall, D. G. Cocks, G. J. Boyle, M. J. Brunger, S. J. Buckman, G. García, Z. Lj. Petrović, J. P. Sullivan, and R. D. White, Plasma Sources Sci. Technol. **26**, 045010 (2017).

[10] R. E. Robson, M. J. Brunger, S. J. Buckman, G. Garcia, Z. Lj. Petrović, and R. D. White, Sci. Rep. **5**, 12674 (2015).

[11] F. Blanco, A. M. Roldán, K. Krupa, R. P. McEachran, R. D. White, S. Marjanović, Z. Lj. Petrović, M. J. Brunger, J. R. Machacek, S. J. Buckman, J. P. Sullivan, L. Chiari, P. Limão-Vieira, and G. García, J. Phys. B: At., Mol. Opt. Phys. **49**, 145001 (2016).

[12] E. K. Anderson, R. A. Boadle, J. R. Machacek, L. Chiari, C. Makochekanwa, S. J. Buckman, M. J. Brunger, G. García, F. Blanco, O. Ingólfsson, and J. P. Sullivan, J. Chem. Phys. **141**, 034306 (2014).

[13] R. D. White, D. Cocks, G. Boyle, M. Casey, N. Garland, D. Konovalov, B. Philippa, P. Stokes, J. de Urquijo, O. González-Magaña, R. P. McEachran, S. J. Buckman, M. J. Brunger, G. Garcia, S. Dujko, and Z. Lj. Petrovic, Plasma Sources Sci. Technol. **27**, 053001 (2018).

[14] M. J. E. Casey, D. G. Cocks, G. J. Boyle, M. J. Brunger, S. Dujko, J. de Urquijo, and R. D. White, Plasma Sources Sci. Technol. **28**, 115005 (2019).

[15] A. Banković, Z. Lj. Petrović, R. E. Robson, J. P. Marler, S. Dujko, and G. Malovi'c, Nucl. Instrum. Methods Phys. Res., Sect. B **267**, 350 (2009).

[16] R. P. McEachran, B. P. Marinković, G. García, R. D. White, P. W. Stokes, D. B. Jones, and M. J. Brunger, J. Phys. Chem. Ref. Data **49**, 013102 (2020).

[17] D. D. Reid and J. M. Wadehra, J. Phys. B: At., Mol. Opt. Phys. **29**, L127 (1996).

[18] W. Tattersall, L. Chiari, J. R. Machacek, E. Anderson, R. D. White, M. J. Brunger, S. J. Buckman, G. García, F. Blanco, and J. P. Sullivan, J. Chem. Phys. **140**, 044320 (2014).

[19] L. Chiari, A. Zecca, S. Girardi, E. Trainotti, G. García, F. Blanco, R. P. McEachran, and M. J. Brunger, J. Phys. B: At., Mol. Opt. Phys. **45**, 215206 (2012).

[20] R. P. McEachran, A. G. Ryman, A. D. Stauffer, and D. L. Morgan, J. Phys. B: At., Mol. Opt. Phys. **10**, 663 (1977).

[21] A. C. L. Jones, C. Makochekanwa, P. Caradonna, D. S. Slaughter, J. R. Machacek, R. P. McEachran, J. P. Sullivan, S. J. Buckman, A. D. Stauffer, I. Bray, and D. V. Fursa, Phys. Rev. A **83**, 032701 (2011).

[22] D. D. Reid and J. M. Wadehra, J. Phys. B: At., Mol. Opt. Phys. **47**, 225211 (2014).

[23] A. Jain, Phys. Rev. A **41**, 2437 (1990).

[24] A. Dalgarno and J. T. Lewis, Proc. R. Soc. London, Ser. A **240**, 284 (1957).

[25] S. Chen, R. P. McEachran, and A. D. Stauffer, J. Phys. B: At., Mol. Opt. Phys. **41**, 025201 (2008).

[26] K. Bartschat, R. P. McEachran, and A. D. Stauffer, J. Phys. B: At., Mol. Opt. Phys. **21**, 2789 (1988).

[27] K. Bartschat, R. P. McEarchran, and A. D. Stauffer, J. Phys. B: At., Mol. Opt. Phys. **23**, 2349 (1990).

[28] R. P. McEachran and A. D. Stauffer, J. Phys. B: At., Mol. Opt. Phys. **46**, 075203 (2013).

[29] D. D. Reid and J. M. Wadehra, J. Phys. B: At., Mol. Opt. Phys. **30**, 2318 (1997).

[30] A. Zecca, L. Chiari, E. Trainotti, D. V. Fursa, I. Bray, A. Sarkar, S. Chattopadhyay, K. Ratnavelu, and M. J. Brunger, J. Phys. B: At., Mol. Opt. Phys. **45**, 015203 (2012).

[31] M. W. J. Bromley (private communication, 2020).

[32] Y. Itikawa, J. Phys. Chem. Ref. Data **46**, 043103 (2017).

[33] R. P. McEachran, F. Blanco, G. García, and M. J. Brunger, J. Phys. Chem. Ref. Data **47**, 033103 (2018).

[34] R. P. McEachran, F. Blanco, G. García, P. W. Stokes, R. D. White, and M. J. Brunger, J. Phys. Chem. Ref. Data **47**, 043104 (2018).

[35] K. R. Hamilton, O. Zatsarinny, K. Bartschat, M. S. Rabasović, D. Šević, B. P. Marinković, S. Dujko, J. Atić, D. V. Fursa, I. Bray, R. P. McEachran, F. Blanco, G. García, P. W. Stokes, R. D. White, D. B. Jones, L. Campbell, and M. J. Brunger, J. Phys. Chem. Ref. Data **50**, 013101 (2021).

[36] G. J. Boyle, W. J. Tattersall, D. G. Cocks, R. P. McEachran, and R. D. White, Plasma Sources Sci. Technol. **26**, 024007 (2017).

[37] R. D. White, R. E. Robson, B. Schmidt, and M. A. Morrison, J. Phys. D: Appl. Phys. **36**, 3125 (2003).

[38] M. J. Brunger, Int. Rev. Phys. Chem. **36**, 333 (2017).